Optical Properties of Bismuth Borate Glasses Doped with Zinc and Calcium Oxides

M. Y. Hassaan[1], H. A. Saudi[2], Hossam M. Gomaa[3, 4], Ammar S. Morsy[4]

1. Physics Dep., Faculty of Science (Males branch), AL Azhar Unvi., Cairo, Egypt
2. Physics Dep., Faculty of Science (Females branch), AL Azhar Unvi., Cairo, Egypt
3. Higher Institute of Engineering, Automotive and Energy, New Heliopolis, Cairo, Egypt
4. Optical Branch, High Institute of Optics technology, Cairo, Egypt

Abstract: Some bismuth-borate oxide glass' samples were prepared by the fast quenching method, where B_2O_3 was replaced with equal concentrations of ZnO and CaO. X-ray diffraction (XRD) was used to examine the internal structure and Fourier transform infrared (FTIR) to identify building units and bonds throughout the studied structural matrices. XRD showed that all samples have short range order structural nature, while FTIR demonstrated some of Zn^{2+} acted as glass network formers and all Bi^{3+} acted as glass. UV-visible measurements and calculations showed a decreasing in the energy band gap from 3.83 eV to 1.73 eV with decreasing B_2O_3 content. Also with decreasing B_2O_3 content, both real refractive index and metallization factor decreased from 3.1 to 1.9 and from 0.56 to 0.71, respectively. For the studied glass' samples, density and molar volume showed inverted behaviors, where the density decreased while the molar volume increases with decreasing B_2O_3.
Keywords: Optics; Linear optics; Glasses; XRD; FTIR; UV-vis.

1. Introduction

Borate glass matrices are of the most used materials in many different fields, because they have the ability to accommodate many of different impurities, so they have a variety of properties depending on the nature of additives/impurities. A lot of authors considered borate glass's matrix a base to develop new compositions have desired properties should be useful to serve Specific application. Generally, there is considerable interest in amorphous/glasses as semiconductors and optical devices because they have a number of interesting physical properties. Oxide glasses containing transition metal cations like Cu, Fe and Zn in multi component glass systems are promising solids for optical applications [1−2]. ZnO is an important additive which act to reduce the melting temperatures in the oxide glass formation process. Zinc borate glasses are very attractive materials, where zinc oxide is considered as n-type semiconductor has a broad optical band gap (up to 3.37 eV) [3] so it has used to improve the glass properties to be useful for many various applications such as photo-voltaic cells, opt-electronic and gas sensors. The interaction of Light with matter is the interaction of the electric field component of light with the matter atoms. Like interaction perturbs the atomic momentum as a result of the polarization process called electronic polarizability of ions. This type of polarizability demonstrates the ease of the deformation of the electronic clouds of applying of an external electromagnetic field. Many properties of the materials such as refraction, electro-optical effect and optical basicity along with optical nonlinearity relate to this interaction/approach [4]. The polarizability approach refers to the electronic polarizability of ions, especially in the field of glass science, like approach has been developed in the most recent publication for more understanding to the optical basicity of oxide glasses [5]. Where the optical nonlinearity result from the electronic polarization of a material when exposed to electromagnetic radiation of high intensity. Numerous oxide glasses were investigated by means of the polarizability approach with an aim to explain the origin of optical nonlinearity. Bismuth borate glasses are of high interest because of their low melting temperatures and their physical stability, also they have high refractive index [6]. Based on the previous publications in the field of oxide glass generally and borate glass especially. The authors tried something different by introduced equal concentration of both ZnO and CaO in the borate glass' matrix. Where ZnO was chosen to modify the optical and structural properties, while CaO was introduced to modify the structural properties, increase the amorphous nature, and help in the melt of both ZnO and Bi_2O_3 and force some of Zn^{2+} cations to share in the glass network as a glass network formers of tetrahedral coordination states. It should take into account, mostly, both ZnO and CaO act as glass network formers and occupied the interstitial vacancies. This means that both of them perturbs the structural properties of borate glasses. Both ZnO and CaO act to reduced BO_4/(BO_4:BO_3) ratio and enhanced the glass' network by increasing

the no. of non-bridging oxygen atoms. Zn and Ca are divalent elements, and their covalent radii are greater than that of B. so it's acceptable to attribute the changes to the presence of CaO, ZnO or both them without any conflict or confusion. The purpose of the present work is to synthesis of some Bismuth Calcium Zinc borate glass' samples and show some of their linear optical parameters.

2. Experimental work

2.1 Glass preparation

High purity materials were used in glasses' preparation process, the purity of each component did reach 99%. Glasses' preparation process was based on the following chemical formula:

$$(58.4 - 2x)mol\% \ B_2O_3 \ . \ (18.8 + x)mol\%ZnO \ . \ (18.8 + x)mol\% \ CaO \ . \ 4mol\%Bi_2O_3$$
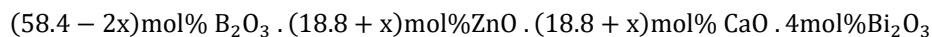
where x = 0, 2, 4, 6 and 8 mol%.

All samples were coded as seen in table 1 which also contains the molar fractions, and molecular weight of each sample. After calculations, each component was Grinded well then weight according to its percentage, after for the components of each sample were mixed well then transferred to porcelain crucibles then melted, at 800 ± 20 °C for 2 h, with frequent stirring to ensure complete homogeneity. Finally, Melts were then rapidly quenched onto pre-cooled copper plates in the air.

Table 1. Samples code, oxides ratios and samples molecular weights

x (mol%)	Ratio of each component in mol%				MW (g/mol)
	B_2O_3	ZnO	CaO	Bi_2O_3	
0.0	58.4	18.8	18.8	4.0	85.14
02	54.4	20.8	20.8	4.0	85.1
04	50.4	22.8	22.8	4.0	85.07
06	46.4	24.8	24.8	4.0	85.03
08	42.4	26.8	26.8	4.0	85

2.2 Glass phase characterization

The obtained solids were characterized X-ray diffraction (XRD) technique using X-ray powder diffractometer (Rigaku Miniflex, Japan, CuKα, λ= 1.5406 Å, radiation in between 2θ = 4° and 2θ = 80°). XRD is a unique powerful technique in detecting the internal structural nature of solid materials, especially in distinguishing between amorphous and crystalline material. However, it was found that the intensity of me seared XRD is affected by instrumental and experimental tools, where it is considered as the number of counts per second, therefore it's more useful to use relative intensity than the absolute one. The relative intensity is obtained by dividing the absolute intensity of every peak by the absolute intensity of the most intense one, and then convert to a percentage, where the most intense peak of a phase is therefore always called the "100% peak", in such case XRD may name as "normalized XRD".

2.3 Structural units identification

FTIR is a good tool for characterizing the glass structure, because each building block and each chemical bond have a unique vibrational frequency considered as its fingerprint, therefore FTIR spectra were used to identify both of the building blocks and chemical bonds within the studied samples, at room temperature, using Fourier transform Infrared (FTIR) spectrometer in the range from 4000 to 400 cm^{-1}. Where, the powdered samples were mixed well with KBr and were then pressed to make pellets suitable for IR measurements. Since, each FTIR band composed of more than one peak, each represents a fixed type of vibration, it should be de-convoluted each band by separating all possible individual peaks, for the current work the bands of FTIR were de-convoluted using origin 8 program which based on Gaussian distribution function

2.4 Optical measurements

Direct and indirect band gap materials became of more interesting materials because of their applications in most modern opt-electronics devices. In the present samples ZnO exists as a fundamental component with different concentration in each glass matrix, since such oxide is considered as non-Centro symmetric compound affected the electronic properties of the studied samples. So, for all studied samples, some linear optical measurements and some other considered by Genway 6405-UV–visible Spectrophotometer which was used to get the optical UV–vis. Spectra, in the range 200 to 2500 nm, at room temperature.

3. Results and discussion

Figures 1a and 1b show as deposited and Normalized XRD for all studied samples, respectively. These figures demonstrated all studied samples did not show any sharp peaks and only two broad humps around 29.5° and 51.8° can be detectable, such humps distinguish non-crystalline solids (amorphous solids). Therefore, it can stated that all studied samples are short range order solids (glass solids) [7-8]. The existence of two humps in XRD as seen in figure 1b may be an indication to formation of two different micro-nucleating agents Zn (about 29.5°) and Bi (about 51.8°) throughout the glass' matrix. As an attempt to get more details, XRD chart for x = 0 was de-convoluted to two separated peaks, based on Lorentz shapes, as seen in figure 2. As seen in table 2, the de-convoluted parameters tell that the peak assigned to Zn is higher and wider than that assigned to Bi, this result is acceptable where the Zn content in all samples is much larger than Bi content. Figure 3 depicts the measured FTIR spectra for the studied samples, where each spectrum shows more than broad band, including those of OH groups' bands, which had cut to improve spectra to be suitable for de-convolution processes as seen in Figure 4 for x=0 sample, all samples were modified by the same way. Table 3 contains the centers of de-convoluted peaks as well as a description for each peak according to previous literatures. Data in table 3 revealed Bi^{3+} and Zn^{+} in octahedral and tetrahedral coordination states, respectively. Hence Bi^{3+} cations occupied the interstitial vacancies as a glass network Modifiers (GNMs), while Zn^{+} cations participated in the glass networks as a glass network formers (GNFs). Also, table 3 showed the presence of BO_3 and BO_4 that are the main structural groups of borate glass. For more interesting study, Authors renormalized the FTIR to clearing and canceling all peaks of weak intensity, as seen in Figure 5, where it's clear that the formalization process produced only two main peaks, distinguished both BO_3 and BO_4 groups. Where it was noticeable that the band of BO_3 is of high intensity while the band of BO_4 is of low intensity. By checking all FTIR for all samples, it was found that with decreasing of B_2O_3 content, the centration of BO_4 decreased while the concentration of BO_3 increased, which may be attributed to the decrease in the relative number of oxygen atoms, as a result to replace rich oxygen oxide (B_2O_3) by boor oxygen oxides (ZnO and CaO). Conversion of BO_4 groups to BO_3 groups means increase in the crystallinity degree in the glass' matrix. Density ρ measurements were carried out, using the fluid displacement method, at room temperature, then used in molar volume V_m calculations. Table 4 depicts the variation of both ρ and V_m with decreasing B_2O_3 content, where they showed invertible behaviors. Such behavior and be explained in the fact that the atomic radii of both Zn^{+} (122 pm) and Ca^{2+} (176pm) cations are much larger than that of B^{3+} (85 pm).
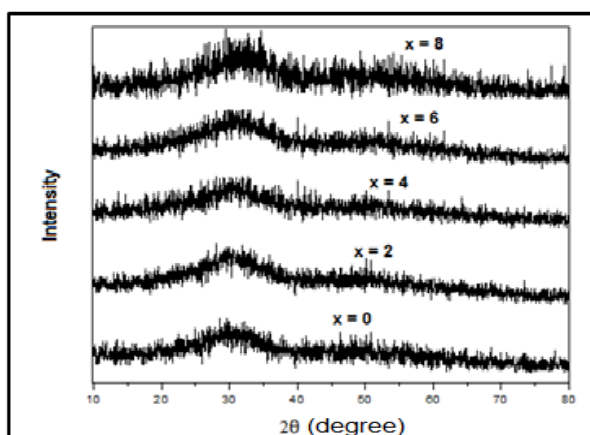
Fig. 1a. As deposited XRD patterns for all samples
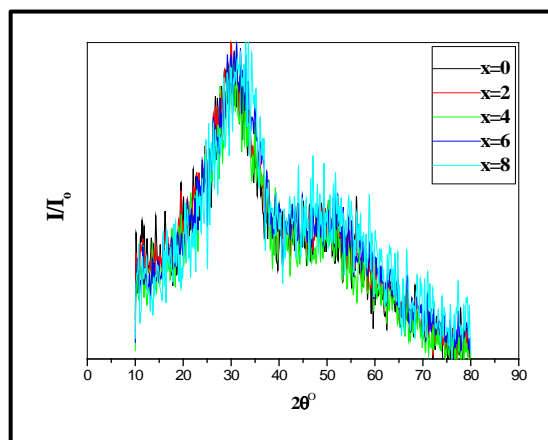
Fig. 1b. Normalized XRD patterns for all samples

Table 2. De-convolution Parameters: area, center, width and height of each peak

Peak	Area	Center	Width	Height
1	16.684	29.473	17.962	0.59133
2	4.4490	51.811	14.535	0.19487

Figure 6 and figure 7 depict measured normalized optical absorption A% and normalized optical trancemittance T%, respectively, in between 290 nm and 750 nm, for all samples. The behavior of both A% and T% with increasing the wavelength of incident photons had been divided in to two regions. In the first region, from 290 nm to 360 nm, A% and T% are constants, approximately, with no observable changes. While in the second region, above 360 nm, A% and T% dispersed with different rates. At UV-edg, A% decreased while T% increased with decreasing B_2O_3 content, as seen in figure 6 and figure 7, respectively. Such fluctuations may attribute to difference

in the sample thickness and/or structural defects. For all samples the absorption coefficient α was calculated using the following relation:

$$\alpha\ (\lambda) = 0.2303\ \frac{A\ (\lambda)}{t}\quad cm^{-1}$$

where A is the normalized absorbance and t is the samples thickness in cm.
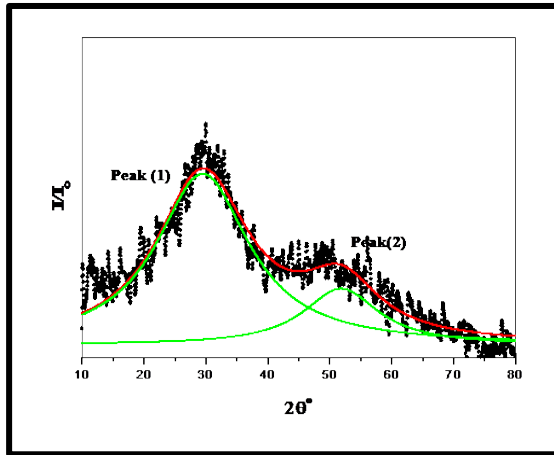
Fig. 2. De-convoluted XRD chart for x = 0
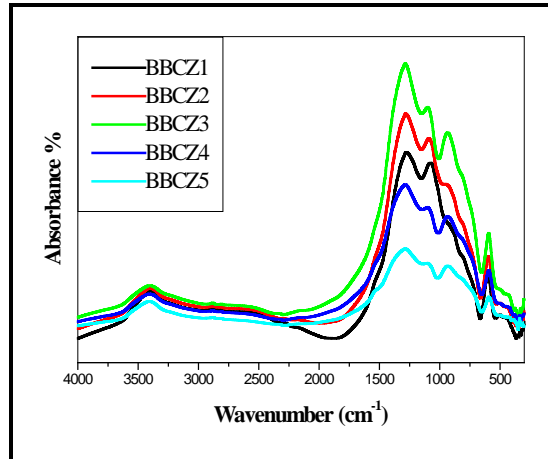
Fig. 3. FTIR spectra for all samples.
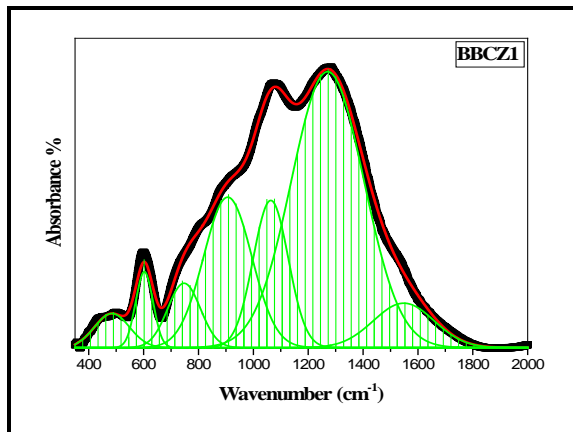
Fig. 4. De-convoluted FTIR spectra for x = 0
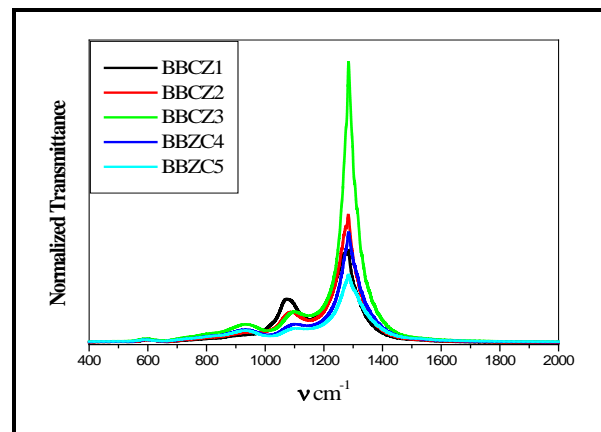
Fig. 5. Normalization FTIR spectra for all samples.

Table 3. FTIR Data: center and assignment of the observed peaks

No.	Peak Center (cm⁻¹)	Assignment	Ref.
1	381	Symmetric stretching vibrations of Bi-O-Bi bonds in pyramidal BiO_6 octahedrons.	[9-10]
2	484	The angle modification of the B-O-B linkages.	[11-12]
3	544	B - O - O in ZnO_4 units	[13-14]
4	660	Bending vibrations of B–O linkage groups.	[15-16]
5	726	BO_3-O-BO_3 bending vibrations.	[17-18]
6	837	Stretching vibrations of B-O bonds in BO_4 units from diborate groups	[19-20]
7	980	Stretching vibrations of B-O in BO_4 units.	[21]
8	1225	Stretching vibrations of B-O bonds in BO_3 units from meta- and ortho-borate groups.	[22-23]

Davis and Motto developed the following mathematical formula to describe the absorption coefficient as a function of both the photon energy hv and the direct/indirect optical band gap E_{opt}.

$$(\alpha h v)^{\xi} = Constant * (h v - E_{Opt})$$

Where $\xi = 2$ for allowing direct transitions and $\xi = \frac{1}{2}$ for allowing indirect transitions [24-25].

Table 4. Density and molar volume for all samples

x (mol%)	ρ (g/cm^3)	Vm (cm^3/mole)
00	3.63	23.45
02	3.52	24.18
04	3.07	27.71
06	2.69	31.61
08	2.45	34.69
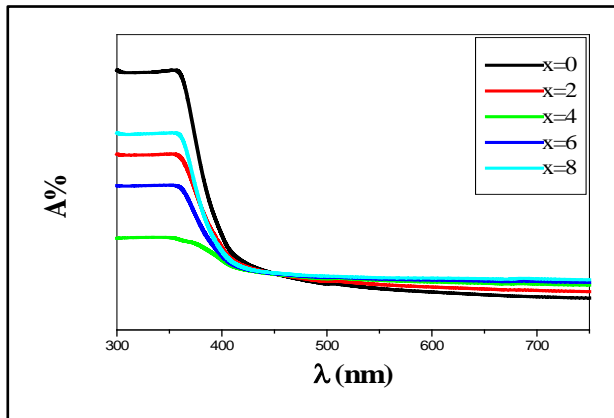
Fig. 6. Optical absorption for all samples
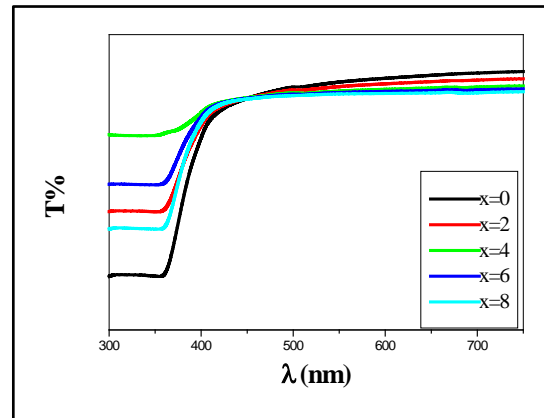
Fig. 7. Optical Transmittance for all samples

The optical band gaps for both direct and indirect transitions can be obtained by plotting $(\alpha h v)^2$ and $(\alpha h v)^{1/2}$ verses hv respectively, then extrapolate the linear portion to intersect the horizontal axis (hv) at point represents the optical band gap [26-27], as seen in the figure 8 and figure 9. For the studied samples, the resulted values for both direct and indirect transitions band gaps were recorded in table 5 which showed the midpoint sample x = 4 to have lowest optical band gaps among the other samples. This result refers that this sample should have lowest absorption and highest transmittance, the thing which appeared clearly in figures 8 and 9. Generally variation of the refractive index n value with respect to wavelength is a sign to the dispersion properties of the material. Where the speed of the light within any material is established by the complex refractive index $n^* = n + iK$ where K is the extinction/attenuation coefficient while n is the refractive index. Physically, K refers to the dissipation of the amplitude of the incident electric field component [28-29]. In other words, the optical characteristics of the material are controlled by the interaction between the electric-field components of the incident light waves and the material atoms/molecules. So 'k' has an important role in describing the light propagation through the material, and determine the amount of the dissipated optical energy (loss energy due the absorption processes). The absorption coefficient α may use to get the extinction coefficient K [19], which depicted in figure 10 for all samples. This figure showed that the contents of both ZnO and CaO did not perturb the Fermi level. The refractive index is an important optical parameter which is sensitive to any fine change in the value of the optical band gap, polarization and internal structure of the solids. In the present work, the following Fresnel's formula was used to calculate the refractive index function n (λ) [30-31].

$$K(\lambda) = \frac{\alpha \lambda}{4\pi}$$

$$R(\lambda) = \frac{[n(\lambda) - 1]^2 + K^2(\lambda)}{[n(\lambda) + 1]^2 + K^2(\lambda)}$$

Figure 11 shows the calculated refractive index function n (λ) for all studied samples, where each chart seems to be composed of three regions:

(i) In the 1st region 290-360 nm the value of the refractive index for each sample exhibit un observable change, the thing which may mean $dn/d\lambda \simeq Zero$.

(ii) While in the 2^{ed} region 360-410 nm (UV region), for each sample, the value of the refractive index decreases linearly ($dn/d\lambda = C_1$).

(iii) Finally, in the 3^{ed} region 410-750 nm (visible region), for each sample, also the value of the refractive index

decreases linearly, $(dn/d\lambda = C_2)$, where $C_2 < C_1$.

In other words, the behavior of refractive index n (λ) with the light wavelength in the range 360 – 410 nm is a normal-dispersion behavior, while in range 410-750 nm samples become non-dispersive. The approximately value of refractive index along the range from 290 to 360 nm is an abnormal behavior may explained from the point of view, the refractive index is a complex quantity consists of real part n (λ) and imaginary part K (λ) where the imaginary part is directly proportion to the wavelength while the real part is inversely proportion with the wavelength. This means that, the rate of change of the real part $dn/d\lambda$ is invert to the rate of change of the imaginary part $dk/d\lambda$. In normal conditions $dn/d\lambda \gg -dk/d\lambda$ [19,30,31]. For any reason, if, $dn/d\lambda = -dk/d\lambda$ the apparent value of the refractive index may does not change as in the present case of the studied glasses in range 290-360 nm. Such phenomena may lead to use materials of similar compositions in many optical, electronic and opt-electronic applications. In the other side, the ZnO content affected the value of the refractive index, the refractive indices for all samples at UV edge were recorded in table 5, where the midpoint sample x = 4 showed the lowest refractive index. The nature of the internal structure of any solid samples may characterized by known its electronic band energy E_g, which correlated to what called metallization (M) which defined as the ratio between the molar refractivity R_m and molar volume Vm [32-33]. The energy gap E_g can be obtained by using Wemple-DiDomenco model (WDD) [34-35] which describes the dispersion in the refractive index as a function in photon energy and the energy band gap, as seen in the following relation. As seen in in figure 12, by plotted $[[n(\lambda)]^2 - 1]^{-1}$ versus $(h\nu)^2$ the slope of the dominating straight line represents $1/2E_dE_g$ while $2E_g/E_d$ the represents the intersected point with the y-axis. Using these two variables the value of the energy gap was obtained for each sample, then reported in table 5. Consequently, these values were used to obtain the Metallization [33] for all studied samples, which are also recorded in table 5.

$$M = \frac{R_m}{V_m} = 1 - \sqrt{\frac{E_g}{20}}$$

$$M \begin{cases} < 1 & non\ metal\ nature \\ \geq 1 & metal\ (crystalline)\ nature \end{cases}$$

$$[[n(\lambda)]^2 - 1]^{-1} = \frac{2E_g}{E_d} + \frac{(h\nu)^2}{2E_dE_g}$$

Metallization values s in table 5 emphasizes what predicted in FTIR section "Conversion of BO_4 groups to BO_3 groups means increase in the crystallinity degree in the glass' matrix". In other word, all the studied samples exhibit amorphous nature, but x = 0 has highest disordered degree.

Table 5. Optical band gaps Eopt, refractive index n and Metallization M

x	E_{Opt}		n	Eg	M
	Direct	Indirect	λ(200nm)		
00	3.09	2.76	3.1	3.83	0.56
02	3.03	2.71	2.5	3.12	0.60
04	2.68	2.37	1.9	3.27	0.60
06	3.00	2.77	2.3	1.96	0.69
08	3.13	2.53	2.7	1.73	0.71
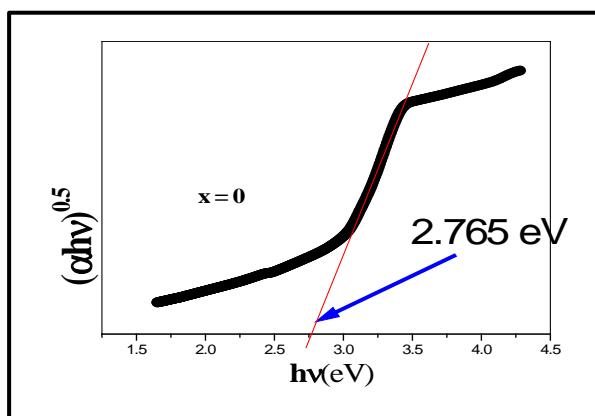
Fig. 8. The absorption coefficient $(\alpha h\nu)^{0.5} \sim$ the phonon energy hν for x = 0
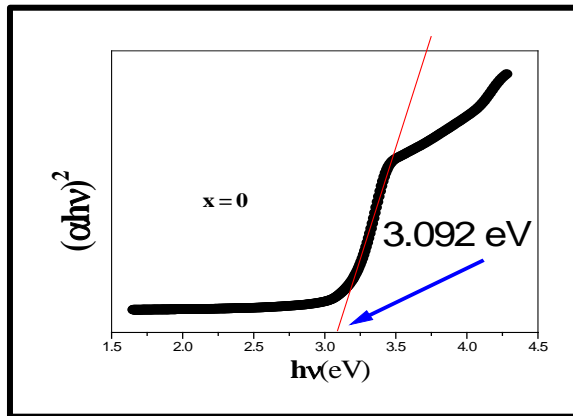
Fig. 9. The absorption coefficient $(\alpha h\nu)^2 \sim$ the phonon energy hν for x = 0
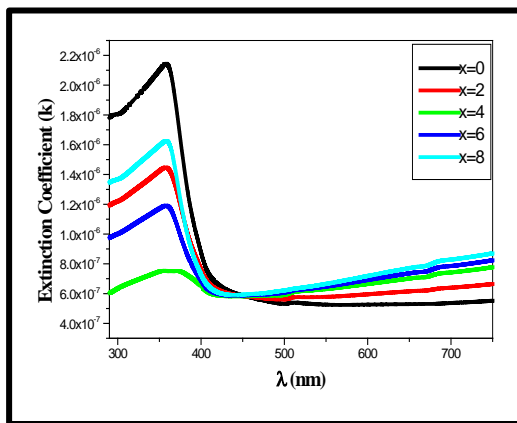
Fig. 10. Extinction coefficient k ~ the phonon wavelength λ for all Samples
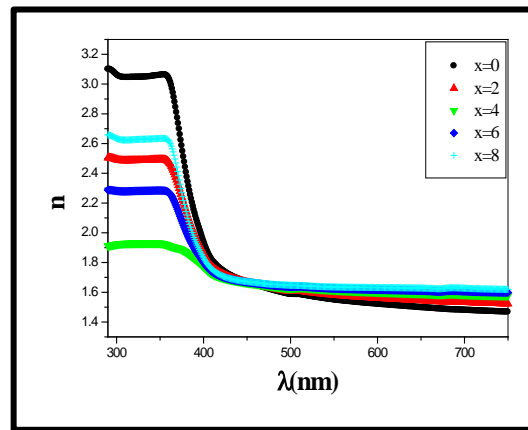
Fig. 11. The Refractive index n ~ phonon wavelength λ for all Samples
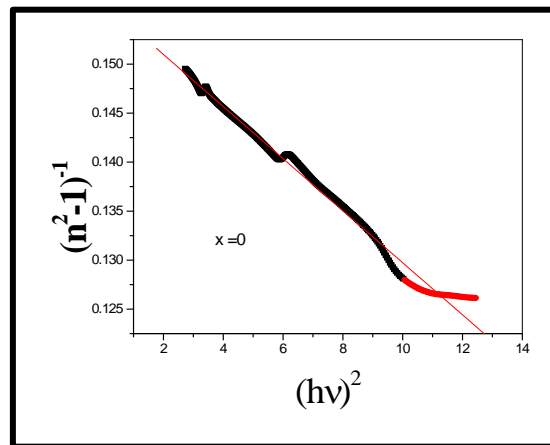
Fig. 12. $[[n(\lambda)]^2 - 1]^{-1}$ ~ $(h\nu)^2$

4. Conclusion

Some bismuth-borate oxide glass' samples were prepared by the fast quenching method, where B_2O_3 was replaced with equal concentrations of ZnO and CaO, according to the following formula:

$$(58.4 - 2x)mol\% \ B_2O_3 \ . \ (18.8 + x)mol\%CaO \ . \ (18.8 + x)mol\%ZnO. \ 4mol\%Bi_2O_3$$
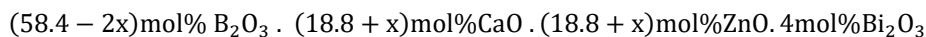
where x = 0, 2, 4, 6 and 8 mol%.

X-ray diffraction (XRD) showed that all samples have short range order structural nature, while Fourier transform infrared (FTIR) demonstrated some of Zn^{2+} acted as glass network formers and all Bi^{3+} acted as glass. UV-visible measurements and calculations showed a decreasing in the energy band gap from 3.83 eV to 1.73 eV with decreasing B_2O_3 content. Also with decreasing B_2O_3 content, both real refractive index and metallization factor decreased from 3.1 to 1.9 and from 0.56 to 0.71, respectively. For the studied glass' samples, density and molar volume showed inverted behaviors, where the density decreased while the molar volume increases with decreasing B_2O_3. Metallization ratio referred that the amorphous nature degree of the studied glasses decreases as both ZnO and CaO contents increase. Systematic analysis of the results suggested that the glass doped with ZnO and CaO concentration may be suitable for display device applications.

5. References

[1] Kaur N, Khanna A, Gónzález-Barriuso M, González F, Chen B. Effects of Al^{3+}, W^{6+}, Nb^{5+} and Pb^{2+} on the structure and properties of borotellurite glasses. Journal of Non-Crystalline Solids. 2015;429:153-163.

[2] Rao SL, Ramadevudu G, Shareefuddin M, Hameed A, Chary MN, Rao ML. Optical properties of alkaline

earth borate glasses. International Journal of Engineering, Science and Technology. 2012;4(4):25-35.

[3]   Ghajari N, Kompany A, Movlarooy T, Roozban F, Majidiyan M. Synthesis, experimental and theoretical investigations of $Zn_{1-x}Cu_xO$ nanopowders. Journal of Magnetism and Magnetic Materials. 2013;325:42-46.

[4]   El-Amir AA, Ohsawa T, Ishii S, Imura M, Segawa H, Sakaguchi I, Nagao T, Shimamura K, Ohashi N. Optoelectronic characteristics of the Ag-doped Si pn photodiodes prepared by a facile thermal diffusion process. AIP Advances. 2019;9(5):055024.

[5]   Tasheva TR, Dimitrov VV. Synthesis, structure and nonlinear optical properties of tellurium oxide–bismuth oxide–boron oxide glasses. Bulgarian Chemical Communications. 2017;49:43-48.

[6]   Dimitrov V, Komatsu T. An interpretation of optical properties of oxides and oxide glasses in terms of the electronic ion polarizability and average single bond strength. J. Univ. Chem. Technol. Metall. 2010;45(3):219-250.

[7]   Lanfredi S, Gênova DH, Brito IA, Lima AR, Nobre MA. Structural characterization and Curie temperature determination of a sodium strontium niobate ferroelectric nanostructured powder. Journal of Solid State Chemistry. 2011;184(5):990-1000.

[8]   Larson AC, Von Dreele RB. General structure analysis system (GSAS). Report LAUR 86-748. Los Alamos National Laboratory. 2000.

[9]   Pasha A, Dayani P, Negalur M, Swamy M, Abhiram J, Rajaramakrishna R. Spectroscopic study of neodymium doped lead-bismuth-borate glasses. In: AIP Conference Proceedings (Vol. 1728, No. 1). AIP Publishing LLC. 2016. p. 020264.

[10]   Bajaj A, Khanna A. Crystallization of bismuth borate glasses. Journal of Physics: Condensed Matter. 2008;21(3):035112.

[11]   Bobkova NM, Trusova EE. Structure of bismuth-borate glasses with RO-group oxides according to IR spectroscopy. Glass and Ceramics. 2015;72:79-82.

[12]   Ibrahim S, Abdel-Baki M, El-Diasty F. Zinc borophosphate glasses for infrared-based optical applications. Optical Engineering. 2012;51(9):093401.

[13]   Saudi HA, Sallam HA, Abdullah K. Borosilicate glass containing bismuth and zinc oxides as a hot cell material for gamma-ray shielding. Physics and Materials Chemistry. 2014;2(1):20-24.

[14]   Colak SC, Akyuz I, Atay F. On the dual role of ZnO in zinc-borate glasses. Journal of Non-Crystalline Solids. 2016;432:406-412.

[15]   Balachander L, Ramadevudu G, Shareefuddin M, Sayanna R, Venudhar YC. IR analysis of borate glasses containing three alkali oxides. ScienceAsia. 2013;39(2):278-283.

[16]   He F, He Z, Xie J, Li Y. IR and Raman spectra properties of Bi_2O_3-ZnO-B_2O_3-BaO quaternary glass system. American Journal of Analytical Chemistry. 2014;5(16):1142-1150.

[17]   Rao PV, Raju GN, Prasad PS, Laxmikanth C, Veeraiah N. Transport and spectroscopic properties of nickel ions in ZnO-B_2O_3-P_2O_5 glass system. Optik. 2016;127(5):2920-2923.

[18]   Gaafar MS, El-Aal NA, Gerges OW, El-Amir G. Elastic properties and structural studies on some zinc-borate glasses derived from ultrasonic, FT-IR and X-ray techniques. Journal of Alloys and Compounds. 2009;475:535-542.

[19]   Saddeek YB, Aly K, Abbady G, Afify N, Shaaban KS, Dahshan A. Optical and structural evaluation of bismuth alumina-borate glasses doped with different amounts of (Y_2O_3). Journal of Non-Crystalline Solids. 2016;454:13-18.

[20]   Sadeq MS, Morshidy HY. Effect of mixed rare-earth ions on the structural and optical properties of some borate glasses. Ceramics International. 2019;45(15):18327-18332.

[21]   Gomaa HM, EL-Dosokey AH. FTIR analysis & dielectric constant for some iron bismuth borate glasses. Drug Designing & Intellectual Properties International Journal. 2018;2(3); 211-214.

[22]   Ali AA, Shaaban HM, Abdallah A. Spectroscopic studies of ZnO borate–tellurite glass doped with Eu_2O_3. Journal of Materials Research and Technology. 2018;7(3):240-247.

[23]   Gautam C, Yadav AK, Mishra VK, Vikram K. Synthesis, IR and Raman spectroscopic studies of (Ba,Sr)TiO_3 borosilicate glasses with addition of La_2O_3.Open Journal of Inorganic Non-metallic Materials. 2012;2:47-54.

[24]   El-Mansy MK, Gomaa HM, Hendawy N, Morsy AS. Effect of exchange of Bi^{+3} by Nb^{+5} on the structural and optical properties of some (BBiNb)$_2$ O_7 CaO oxide glasses. Journal of Non-Crystalline Solids. 2018;485:42-46.

[25]   Kotbi A, Hartiti B, Fadili S, Ridah A, Thevenin P. Some physical parameters of CuInGaS_2 thin films deposited by spray pyrolysis for solar cells. Applied Physics A. 2017;123(5):379.

[26]   Algarni H, Reben M, AbouDeif YM, Damak K, Assadi AA, Maâlej R, Yousef ES. Thermal and spectroscopic properties of high dense optical glasses TeO2–Bi_2O_3–WO_3 (TBW) doped with Er_2O_3 as laser material. Science of Advanced Materials. 2018;10(6):818-826.

[27]   Malchukova EV, Nepomnyashchikh AI, Boizot B, Terukov EI. Radiation effects and optical properties of aluminoborosilicate glass doped with RE ions. Glass Physics and Chemistry. 2018;44(4):356-363.

[28] Abbady GH, Aly KA, Saddeek Y, Afifiy N. Linear and non-linear optical properties of amorphous Se and M_5Se_{95} (M= Ge, Ga and Zn) films. Bulletin of Materials Science. 2016;39(7):1819-1825.

[29] Ebisawa F, Hoshino M, Sukegawa K. Self-holding photochromic polymer Mach–Zehnder optical switch. Applied physics letters. 1994;65(23):2919-2921.

[30] El Nahrawy AM, Moez AA, Saad AM. Sol-gel preparation and spectroscopic properties of modified sodium silicate/tartrazine dye nanocomposite. Silicon. 2018;10(5):2117-2122.

[31] Ganesh V, Yahia IS, AlFaify S, Shkir M. Sn-doped ZnO nanocrystalline thin films with enhanced linear and nonlinear optical properties for optoelectronic applications. Journal of Physics and Chemistry of Solids. 2017;100:115-125.

[32] Boda R, Shareefuddin M, Chary MN, Sayanna R. FTIR and optical properties of europium doped lithium zinc bismuth borate glasses. Materials Today: Proceedings. 2016;3(6):1914-1922.

[33] Thakur V, Singh A, Punia R, Kaur M, Singh L. Effect of BaTiO3 on the structural and optical properties of lithium borate glasses. Ceramics International. 2015;41(9):10957-10965.

[34] Ou K, Wang S, Bai L, Wang Y, Zhang K, Yi L. Investigation on annealing temperature-dependent optical properties of electron beam evaporated ZnSe thin films. Thin Solid Films. 2019;669:247-252.

[35] Maghanga C. Influence of deposition parameters on the optical properties of sputtered tungsten oxide films. Int. J. Thin Films Sci.Technol. 2018;7(2):61–65.